Preparation, Structure, and Divergent Fluxional Behavior of Cationic Dinuclear Iron Acetylides $[Fp^*_2(C{\equiv}C{-}R)]BF_4$ (R = H, Ph)

Munetaka Akita,* Masako Terada, Shuji Oyama, and Yoshihiko Moro-oka*

Research Laboratory of Resources Utilization, Tokyo Institute of Technology, 4259 Nagatsuta, Midori-ku, Yokohama 227, Japan

Received August 14, 1989

Cationic diiron μ-acetylide complexes $[FP_2(C{\equiv}C{-}R)]BF_4$ [**2a**, FP_2 = Fp^*_2, R = H; **2b**, FP_2 = Fp^*_2, R = Ph; **2c**, FP_2 = Fp*Fp, R = Ph; **2d**, Fp_2, R = Ph; FP = $(\eta^5\text{-}C_5Me_5)Fe(CO)_2$ (Fp*), $(\eta^5\text{-}C_5H_5)Fe(CO)_2$ (Fp)] are prepared by the ligand-exchange reaction of $[FP^+(THF)]BF_4$ with FP—C≡C—R (**1a**, FP = Fp*, R = H; **1b**, FP = Fp*, R = Ph; **1c**, FP = Fp, R = Ph). Molecular structures of **1a**, **1b**, **2a**, and **2b** were determined by single-crystal X-ray diffraction studies. Spectroscopic analyses of **2** reveal the dominant contribution of a π-complex resonance form, $(\eta^2\text{-M}{-}C{\equiv}C{-}R)M^+$ (A), as well as fluxional behavior. For $[Fp^*_2(C{\equiv}C{-}H)]BF_4$ (**2a**) the ^{13}C NMR absorptions of the two ethynyl carbon atoms, distinctively observed at lower temperature (<−60 °C), emerge as a single absorption with the averaged δ and J_{CH} values for the α and β carbons in the limiting spectrum accompanied by coalescence of the Fp* signals at 50 °C. The H atom on the ethynyl ligand moves between the two ethynyl carbon atoms faster than the NMR time scale at higher temperature. On the other hand, $[FP_2(C{\equiv}C{-}Ph)]BF_4$ (**2b–d**) does not show any notable changes over the range of −80 to +30 °C except for the coalescence of the FP signals. The transition states of these processes correspond to the limiting resonance structures

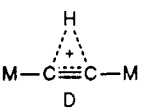

D

for **2a** and M—C(M)=C⁺—Ph (C) for **2b–d**. As is evident from the molecular structure of **2a** and **2b**, the π-bonded metal atom lies closer to the β-carbon atom of the acetylide part than the α-carbon atom, in contrast to the previously reported μ-acetylide complexes. The structural feature arises from the additional contribution of a vinylidene complex resonance form, $M^+{=}C{=}C(M)R$ (B), as well as the absence of structural constraints owing to bridging ligands or a metal–metal bond. Thus, spectroscopic and crystallographic analyses reveal the contribution of B in addition to the dominant contribution of A, and through analyses of dynamic processes the contribution of C or D becomes apparent. The present work suggests that a 1,2-H shift mechanism similar to that proposed for the fluxional process of **2a** operates for the formation of a vinylidene complex from a terminal acetylene and a metal complex.

Introduction

Extensive studies have focused on the chemical behavior of transition-metal complexes bearing a C≡C functional group, that is, metal acetylides (M—C≡C—R) and η^2-acetylene complexes [M(R—C≡C—R)].[1] The acetylide ligands are isoelectronic with CO, CN^-, and CNR and can be converted to vinylidene and acyl ligands.[2] On the other hand, acetylenes have been widely used as a classical two-electron-donating π-acidic ligand. "Umpolung" of inherently electron-rich acetylenes is realized by coordination to a cationic transition-metal center, and cationic η^2-acetylene complexes $[M^+(R{-}C{\equiv}C{-}R)]$ are susceptible to nucleophilic attack to give η^1-vinyl complexes. This transformation has become a promising synthetic route for functionalized alkenes.[3]

Dinuclear μ-acetylide complexes[4] (hybrids of the above-mentioned two coordination modes), in which the acetylide ligand is bound to one metal center in a η^1 fashion (σ-bonded) and to the other metal center in a η^2 fashion (π-bonded), have also attracted much attention as a model for surface-bound species. Oscillation of the bridging acetylide ligands between two metal centers like a wiper often results in fluxional behavior.

However, most studies have dealt with complexes bearing a substituent at the β carbon of the acetylide ligands, and little information is available on the chemical behavior of the parent acetylide ligand, i.e., the ethynyl

(1) Collman, J. P.; Hegedus, L. S.; Norton, J. R.; Finke, R. G. *Principles and Applications of Organotransition Metal Chemistry*; University Science Book: Mill Valley, CA, 1987.

(2) (a) Nast, R. *Coord. Chem. Rev.* **1982**, *47*, 89. (b) Bruce, M. I.; Swincer, A. G. *Adv. Organomet. Chem.* **1983**, *22*, 59. (c) Jolly, P. W.; Pettit, R. *J. Organomet. Chem.* **1968**, *12*, 491. (d) Davison, A.; Selegue, J. P. *J. Am. Chem. Soc.* **1978**, *100*, 7763. (e) Davison, A.; Solar, J. P. *J. Organomet. Chem.* **1978**, *155*, C8. (f) Adams, R. D.; Davison, A.; Selegue, J. P. *J. Am. Chem. Soc.* **1979**, *101*, 7232. (g) Davison, A.; Selegue, J. P. *Ibid.* **1980**, *102*, 2455. (h) Boland, B. E.; Fam, S. A.; Hughes, R. P. *J. Organomet. Chem.* **1979**, *172*, C29. (i) Boland-Lussier, B. E.; Churchill, M. R.; Hughes, R. P.; Rheingold, A. L. *Organometallics* **1982**, *1*, 628. (j) Boland-Lussier, B. E.; Hughes, R. P. *Ibid* **1982**, *1*, 635. (k) Folting, K.; Huffman, J. C.; Lewis, L. N.; Caulton, K. G. *Inorg. Chem.* **1979**, *18*, 3483. (l) Lewis, L. N.; Huffman, J. C.; Caulton, K. G. *J. Am. Chem. Soc.* **1980**, *102*, 403. (m) Pourreau, D. B.; Geoffroy, G. L.; Rheingold, A. L.; Geib, S. J. *Organometallics* **1986**, *5*, 1337. (n) Senn, D. R.; Wong, A.; Patton, A. T.; Marsi, M.; Strouse, C. E.; Gladysz, J. A. *J. Am. Chem. Soc.* **1988**, *110*, 6096.

(3) Reger, D. L. *Acc. Chem. Res.* **1988**, *21*, 229 and references cited therein.

(4) (a) Carty, A. J. *Pure Appl. Chem.* **1982**, *54*, 113. (b) Sappa, E.; Tiripicchio, A.; Braunstein, P. *Chem. Rev.* **1983**, *83*, 203. (c) Abu Salah, O. M.; Bruce, M. I. *J. Chem. Soc., Dalton Trans.* **1974**, 2302, 2311. (d) Ciriano, M.; Howard, J. A. K.; Spencer, J. L.; Stone, F. G. A.; Wadepohl, H. *Ibid.* **1979**, 1749. (e) Kolobova, N. E.; Skipkin, V. V.; Rozantseva, T. V.; Struchkov, Yu. T.; Aleksandorov, G. G.; Andrianov, V. G. *J. Organomet. Chem.* **1981**, *218*, 351. (f) Hutten, A. T.; Shebanzadeh, B.; Shaw, B. L. *J. Chem. Soc., Chem. Commun.* **1984**, 549. (g) Hutten, A. T.; Langrick, C. R.; McEwan, D. M.; Pringle, P. G.; Shaw, B. L. *J. Chem. Soc., Dalton Trans.* **1985**, 2121. (h) Deraniyagala, S. P.; Grundy, K. R. *Organometallics* **1985**, *4*, 424. (i) Cowie, M.; Loeb, S. J. *Ibid.* **1985**, 852. (j) Carriedo, G. A.; Miguel, D.; Riera, V.; Solans, X.; Font-Altaba, M.; Coll, M. *J. Organomet. Chem.* **1986**, *299*, C43. (k) Seyferth, D.; Hoke, J. B.; Wheeler, D. R. *J. Organomet. Chem.* **1988**, *341*, 421. (l) Erker, G.; Fromberg, W.; Benn, R.; Mynott, R.; Angermund, K.; Kruger, C. *Organometallics* **1989**, *8*, 911.

0276-7333/90/2309-0816$02.50/0

(C≡C—H) ligand.[2a,5] In this paper we report preparation of cationic diiron μ-acetylide complexes with the parent ethynyl ligand, $[Fp^*_2(C{\equiv}C{-}H)]BF_4$ (**2a**), and with the phenylethynyl ligand, $[Fp^*_2(C{\equiv}C{-}Ph)]BF_4$ (**2b**), $[FpFp^*(C{\equiv}C{-}Ph)]BF_4$ (**2c**), and $[Fp_2(C{\equiv}C{-}Ph)]BF_4$ (**2d**), from the appropriate mononuclear iron acetylide complexes Fp*—C≡C—H (**1a**), Fp*—C≡C—Ph (**1b**), and Fp—C≡C—Ph (**1c**). Variable-temperature NMR analyses reveal divergent fluxional behavior for **2a** and **2b–d**. In addition, the molecular structures of **1a**, **1b**, **2a**, and **2b** are determined by single-crystal X-ray diffraction studies.

Results

Preparation of Mononuclear Acetylide (1) and Cationic Dinuclear (2) Iron μ-Acetylide Complexes. Mononuclear acetylide complexes (**1a** and **1b**) were prepared in a manner similar to the preparation of Fp—C≡C—Ph (**1c**),[6] i.e., metathesis between Fp*I and alkali-metal acetylide, and were isolated as orange-yellow crystals in moderate yields after column chromatography on alumina (eq 1).

$$Fp^*{-}I + LiC{\equiv}C{-}R \xrightarrow[THF]{} Fp^*{-}C{\equiv}C{-}R \quad (1)$$
$$R = H\ (\mathbf{1a}),\ 42\%$$
$$R = Ph\ (\mathbf{1b}),\ 65\%$$

Treatment of the resulting mononuclear acetylide complexes (**1**) with labile iron cations $[FP^+(THF)]BF_4$ [FP: $(\eta^5\text{-}C_5Me_5)Fe(CO)_2$ (Fp*) and $(\eta^5\text{-}C_5H_5)Fe(CO)_2$ (Fp)][7] in CH_2Cl_2 readily afforded cationic dinuclear μ-acetylide complexes (**2**) as dark yellow to organe-red crystals after crystallization from a mixture of dichloromethane and ether (eq 2). Both the reaction of **1b** with $[Fp^+(THF)]BF_4$ and the reaction of **1c** with $[Fp^{*+}(THF)]BF_4$ afforded the spectroscopically identical product (**2c**).

$$\underset{\mathbf{1}}{FP{-}C{\equiv}C{-}R} + [FP^+(THF)]BF_4 \xrightarrow[CH_2Cl_2]{} [FP_2(C{\equiv}C{-}R)]BF_4 \quad (2)$$
$$FP_2 = Fp^*_2,\ R = H\ (\mathbf{2a}),\ 82\%$$
$$FP_2 = Fp^*_2,\ R = Ph\ (\mathbf{2b}),\ 82\%$$
$$FP_2 = Fp^*Fp,\ R = Ph\ (\mathbf{2c}),\ 68\%\ \text{from}\ \mathbf{1b},\ 73\%\ \text{from}\ \mathbf{1c}$$
$$FP_2 = Fp_2,\ R = Ph\ (\mathbf{2d}),\ 56\%$$

Characterization of Mononuclear Acetylide Complexes 1. The structure of **1** was characterized by ^1H and ^{13}C NMR, IR, and X-ray crystallography (Tables I and II).

Spectroscopic features of the Fp* part are similar to those of Fp*-alkyl complexes. ν_{C-H} absorption (3281 cm^{-1}) at higher frequencies observed for **1a** and $\nu_{C\equiv C}$ absorptions clearly indicates the presence of alkynyl ligands,[8] while $\nu_{C\equiv C}$ could not be observed for **1a**. Both carbon resonances of the ethynyl group in **1a** appear in the same region and are readily assigned on the basis of the J_{CH} value. The ethynyl carbon atoms in **1b** are observed at lower field than those of **1a**. Since the resonance at 112.50 ppm (**1b**) is broadened by long-range coupling when measured in a gated decoupled mode, it is tentatively assigned to C_β. This assignment is supported by comparison with the spectra of **1c**, for which signals could be unequivocally assigned on the basis of ^{13}C–^{57}Fe coupling constants.[9]

The molecular structures of **1a** and **1b** were determined by X-ray crystallography. The structure of **1c** already has been reported.[10] Crystallographic data, positional parameters, and selected bond lengths and angles are listed in Tables III–VII. ORTEP drawings for **1a** and **1b** are reproduced in Figures 1 and 2. To our knowledge **1a** is the first example of a structurally characterized parent

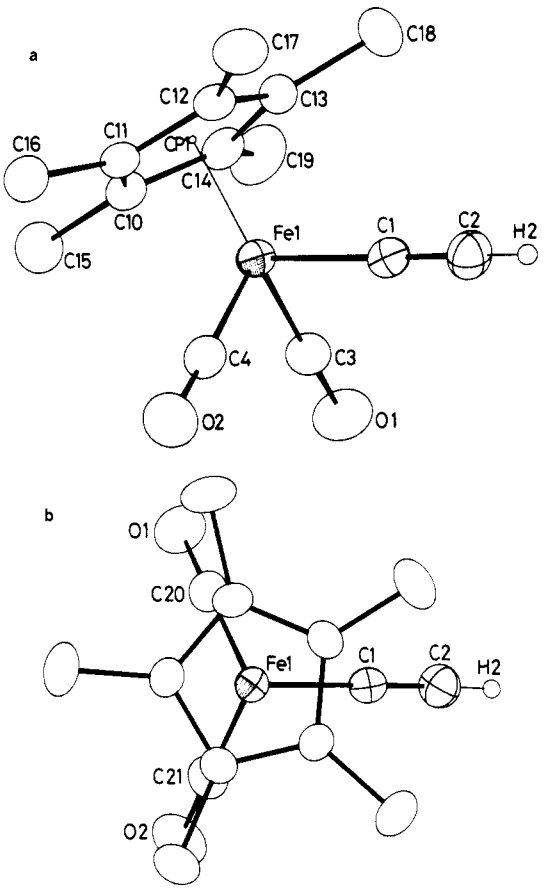

Figure 1. Molecular structure of Fp*—C≡C—H (**1a**) drawn at the 30% probability level: (a) perspective view; (b) top view.

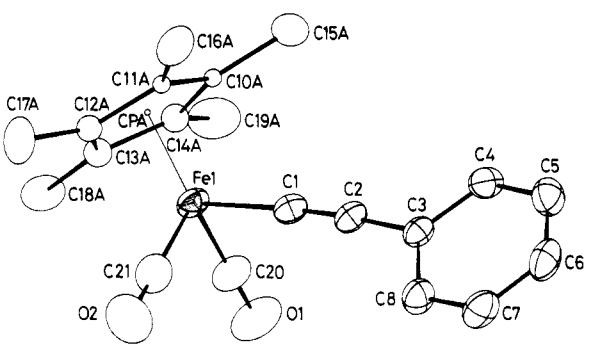

Figure 2. Molecular structure of Fp*—C≡C—Ph (**1b**) drawn at the 30% probability level. For the disordered part only the dominant contributors are reproduced.

(5) (a) Yamazaki, H.; Nishido, Y.; Matsumoto, Y.; Sumida, S.; Hagihara, N. *J. Organomet. Chem.* **1966**, *6*, 86. (b) Kim, P. J.; Masai, H.; Sonogashira, K.; Hagihara, N. *Inorg. Nucl. Chem. Lett.* **1970**, *6*, 181. (c) Sonogashira, K.; Yatake, T.; Tohda, Y.; Takahashi, S.; Hagihara, N. *J. Chem. Soc., Chem. Commun.* **1977**, 291. (d) Sonogashira, K.; Fujikura, Y.; Yatake, T.; Toyoshima, N.; Takahashi, S.; Hagihara, N. *J. Organomet. Chem.* **1978**, *145*, 101. (e) Bell, R. A.; Chisholm, M. H.; Cough, D. A.; Rankel, L. A. *Inorg. Chem.* **1977**, *16*, 677. (f) Appel, M.; Heidrich, J.; Beck, W. *Chem. Ber.* **1987**, *120*, 1087. (g) Nast, R.; Schneller, P.; Hengefeld, A. *J. Organomet. Chem.* **1981**, *214*, 273. (h) Cross, D. J.; Davison, M. F. *J. Chem. Soc., Dalton Trans.* **1986**, 411.

(6) Green, M. L. H.; Mole, T. *J. Organomet. Chem.* **1968**, *12*, 404.

(7) (a) Reger, D. L.; Colemman, C. *J. Organomet. Chem.* **1977**, *131*, 153. (b) Cathline, D.; Astruc, D. *Organometallics* **1984**, *3*, 1094. (c) Akita, M.; Kawahara, T.; Terada, M.; Kakinuma, N.; Moro-oka, Y. *Ibid.* **1989**, *8*, 687.

(8) Pletsch, E.; Seibl, J.; Simon, W.; Clerc, T. *Strukturäufklarung organischer Verbindungen*; Springer: Heidelberg, 1981.

(9) Koridze, A. A.; Astakhova, N. M.; Petrovskii, P. V. *J. Organomet. Chem.* **1983**, *254*, 354.

(10) Goddard, R.; Howard, J.; Woodward, P. *J. Chem. Soc., Dalton Trans.* **1974**, 2025.

Table I. ^{1}H NMR[a] and IR Data for 1 and 2

	^{1}H NMR, ppm				IR, cm^{-1}			
complex	solvent	temp, °C	*R*	Cp or Cp*	solvent	C–H	C≡C	C≡O
1a	C_6D_6	27	1.99	1.44	KBr	3281		2005, 1966
					CH_2Cl_2	3273		2019, 1968
1b	C_6D_6	27	7.04–7.33	1.88	KBr		2094	2006, 1945
					CH_2Cl_2		2095	2013, 1966
1c	$CDCl_3$[b]		7.3	5.05	KBr		2104	2033, 1990
					CH_2Cl_2		2104	2038, 1989
2a	CD_2Cl_2	27	3.76	1.81	KBr	3156	1809	2048, 2015
		−80	3.66	1.80				1981, 1959
					CH_2Cl_2		1788	2030 (sh), 2024
								1991, 1980 (sh)
2b	CD_2Cl_2	27	7.38–7.57	1.70	KBr		1869	2028, 2001
		−80	7.3–7.6	1.74				1981, 1968
					CH_2Cl_2			2020, 1990
								1976
2c	acetone-d_6	27	7.38–7.72	1.89 5.57	KBr		1863	2055, 2029
		−90	7.4–7.7	1.91 5.71				1997, 1957
				1.98 5.80	CH_2Cl_2			2055, 2030
								1983
2d	acetone-d_6	27	7.41–7.74	5.70	CH_2Cl_2			2057, 2045
		−80	7.4–7.7	5.81				2010, 1996
				5.98				

[a] Observed at 100 MHz. [b] See ref 6.

Table II. ^{13}C NMR Data (ppm) for 1 and 2[a]

complex	solvent	temp, °C	Fe–C≡C–R		Cp* or Cp		CO
1a	C_6D_6	27	96.99 (d, 55.0)	97.49 (d, 227.4)	9.62 (q, 128.1)	96.72	215.54
1b	$CDCl_3$	27	105.84	112.50	9.84 (q, 128.2)	96.95	214.56
1c[b]	CH_2Cl_2		89.8	116.3	85.6		213.0
2a	$CDCl_3$	50	103.45 (d, 128)		9.47 (q, 128.9)	99.61	213.54
	CD_2Cl_2	−90	124.18 (d, 29.7)	72.22 (d, 227.0)	10.09 (q, 128.9)	99.58	213.86
						99.97	215.06
2b	CD_2Cl_2	27	109.27	85.74	9.88 (q, 128.9)	100.87	214.95
	CD_2Cl_2	−80	107.28	84.98	10.06	100.08	212.29
					10.17	100.89	214.37
							215.06
							218.32
2c	acetone-d_6	27	96.60	91.17	9.97 (q, 129.1)	101.27	212.80
							214.86
2d	acetone-d_6	27	86.51	74.82	89.37 (d, 184.7)		212.21
		−80	[c]	75.60	88.60		211.25
					90.15		212.25
							212.96 (br)

[a] Observed at 68 MHz. [b] See ref 9. [c] Not located owing to overlapping with the Cp* signals. Acetylide carbon signals of **2b–d** are tentatively assigned. Ph signals: **1b**: 124.52 (dt, 167.4, 7.7, p), 127.63 (dd, 167.4, 7.7, o), 128.62 (ipso), 131.12 (dt, 160.8, 6.6, m). **1c**: 125.3, 128.1, 131.2. **2b** (at 27 °C) 127.97 (t, 8.2, ipso), 128.56 (dt, 163.1, 8.5, p), 129.60 (dd, 162.0, 7.7, o), 131.56 (dt, 159.8, 6.8, m); (at −80 °C) 127.41, 128.05, 129.27, 131.57. **2c**: 128.97 (dt, 162.9, 7.1, p), 129.56 (t, 7.7, ipso), 130.08 (dd, 162.9, 7.7, o), 132.43 (dt, 162.8, 7.1, m). **2d** (at 27 °C) 128.82 (dt, 161.5, 7.7, p), 128.99 (t, 7.7, ipso), 129.88 (dd, 162.9, 7.7, o), 132.84 (dt, 162.8, 7.1, m); (at −80 °C) 128.50, 128.75, 129.69, 132.96.

Table III. Crystallographic Data

	1a	**1b**	**2a**	**2b**
formula	$C_{14}H_{16}O_2Fe$	$C_{20}H_{20}O_2Fe$	$C_{26}H_{31}O_4Fe_2BF_4$	$C_{32}H_{35}O_4Fe_2BF_4$
fw	272.12	384.21	606.04	682.10
space group	$P2_1/n$	$Pccn$	$P2_1/a$	$P2_1/a$
a/Å	14.464 (3)	15.141 (2)	15.152 (2)	13.537 (4)
b/Å	7.952 (1)	15.875 (2)	16.855 (1)	26.523 (3)
c/Å	12.253 (3)	14.885 (2)	11.983 (2)	8.795 (2)
β/deg	108.29 (3)		112.667 (9)	98.38 (2)
Z	4	8	4	4
V/Å^3	1338.1 (5)	3577.8 (8)	2823.8 (6)	3124.2 (11)
d_{calc}	1.351	1.293	1.426	1.451
cryst size	0.2 × 0.2 × 0.3	0.05 × 0.05 × 0.3	0.2 × 0.2 × 0.2	0.05 × 0.2 × 0.5
μ/cm^{-1}	10.510	7.942	10.181	9.249
2θ/deg	2–55	2–50	2–55	2–57
unique data with $F > 3\sigma$	2489	2009	3584	5285
no. of variables	233	287	479	453
data/variables	11.7	7.0	7.5	11.7
p	0.002	0.02	0.006	0.006
R[a]	0.0358	0.0703	0.0512	0.0790
R_w[b]	0.0309	0.0830	0.0388	0.0785

[a] $R = \sum(|F_o| - |F_c|)/\sum|F_o|$. [b] $R_w = [\sum w(|F_o| - |F_c|)^2/\sum w|F_o|^2]^{1/2}$.

Table IV. Positional Parameters and B_{eq} (Å²) for Non-Hydrogen atoms of Fp*—C≡C—H (1a)

atom	x	y	z	B_{eq}
Cp1[a]	0.02720	0.61514	0.82915	
Fe1	0.02861 (2)	0.80223 (5)	0.75807 (2)	3.11 (1)
C1	0.1193 (2)	0.9777 (4)	0.8272 (2)	3.62 (8)
C2	0.1757 (2)	1.0827 (4)	0.8709 (3)	4.8 (1)
C3	−0.0665 (2)	0.9492 (4)	0.7186 (3)	4.15 (9)
C4	0.0581 (2)	0.8228 (4)	0.6303 (3)	4.24 (9)
C10	−0.0435 (2)	0.5714 (3)	0.7511 (2)	3.45 (8)
C11	0.0556 (2)	0.5402 (3)	0.7596 (2)	3.34 (8)
C12	0.1152 (2)	0.6151 (3)	0.8630 (2)	3.27 (7)
C13	0.0532 (2)	0.6887 (4)	0.9206 (2)	3.45 (7)
C14	−0.0444 (2)	0.6603 (3)	0.8515 (2)	3.69 (8)
C15	−0.1307 (3)	0.5043 (5)	0.6582 (3)	5.4 (1)
C16	0.0894 (3)	0.4360 (4)	0.6777 (3)	5.1 (1)
C17	0.2246 (2)	0.6101 (5)	0.9074 (3)	5.0 (1)
C18	0.0848 (3)	0.7709 (5)	1.0358 (3)	5.6 (1)
C19	−0.1341 (3)	0.7077 (5)	0.8824 (4)	6.4 (1)
O1	−0.1291 (2)	1.0442 (3)	0.6946 (2)	6.72 (9)
O2	0.0784 (2)	0.8330 (3)	0.5471 (2)	7.15 (9)

[a] Cp1 is the centroid of C10–C14.

Table V. Selected Bond Lengths and Angles for Fp*—C≡C—H (1a)[a]

	Bond Lengths, Å		
Fe1–Cp1	1.727 (0)	C2–H2	0.865 (33)
Fe1–C1	1.921 (3)	C3–O1	1.145 (4)
Fe1–C3	1.754 (3)	C4–O2	1.149 (4)
Fe1–C4	1.755 (3)	C–C(C10–C14)	1.423
Fe1–(C10–C14)	2.109	C(C10–C14)–Me	1.502
C1–C2	1.173 (4)		
	Bond Angles, deg		
Cp1–Fe1–C1	121.21 (8)	C1–C2–H2	177.7 (24)
Cp1–Fe1–C3	125.49 (12)	Fe1–C3–O1	178.69 (31)
Cp1–Fe1–C4	125.08 (10)	Fe1–C4–O2	178.57 (29)
C1–Fe1–C3	90.33 (13)	C–C–C(C10–C14)	107.99
C1–Fe1–C4	90.10 (13)	C–C(C10–C14)–Me	125.93
Fe1–C1–C2	178.70 (26)		

[a] Lengths and angles without standard deviations are averaged values. Cp1 is the centroid of C10–C14.

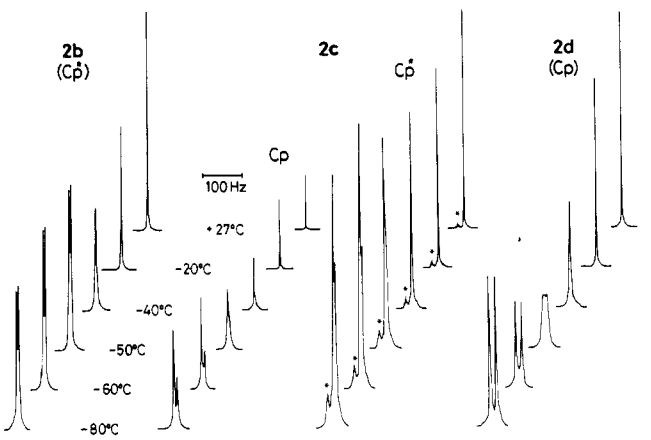

Figure 3. Variable-temperature ^{1}H NMR spectra of **2b** (in CD_2Cl_2), **2c** (in acetone-d_6), and **2d** (in acetone-d_6) observed at 100 MHz. Only Cp and Cp* parts are reproduced. The resonances denoted by asterisks represent the residual proton of the solvent.

acetylide complex. The structure of Fp* parts in **1a** and **1b** is a typical three-legged piano-stool structure, and no significant difference is observed compared with previously reported Fp*–alkyl and –acyl complexes.[11] The Fe—C≡C angle in **1a–c** is virtually 180°, and the Fe–C [1.921 Å (**1a**), 1.924 Å (**1b**), 1.920 Å (**1c**)] and the C≡C bond lengths [1.173 Å (**1a**), 1.214 Å (**1b**), 1.201 Å (**1c**)] are essentially the same regardless of substituents and ligands. The C≡C lengths fall in the range of those of organic acetylenes (ca. 1.20 Å)[12] and organometallic acetylides (1.18–1.25 Å).[2a]

(11) (a) Wright, M. E.; Nelson, G. O.; Glass, R. S. *Organometallics* **1985**, *4*, 245. (b) Akita, M.; Kondoh, A.; Moro-oka, Y. *J. Chem. Soc., Dalton Trans.* **1989**, 2025.

Table VI. Positional Parameters and B_{eq} (Å²) for Non-Hydrogen Atoms of Fp*—C≡C—Ph (1b)[a]

atom	x	y	z	B_{eq}
CpA	1.00259	0.13256	0.70801	
CpB	1.00008	0.12733	0.71082	
Fe1	0.97757 (6)	0.17971 (5)	0.80995 (6)	3.76 (2)
C1	1.0561 (4)	0.2569 (4)	0.8695 (4)	3.7 (2)
C2	1.1010 (4)	0.3078 (4)	0.9096 (4)	3.7 (2)
C3	1.1478 (4)	0.3718 (4)	0.9578 (4)	3.3 (2)
C4	1.2396 (5)	0.3728 (4)	0.9645 (5)	4.2 (2)
C5	1.2825 (5)	0.4380 (5)	1.0082 (5)	5.1 (2)
C6	1.2355 (6)	0.5033 (5)	1.0463 (5)	5.2 (2)
C7	1.1457 (6)	0.5016 (5)	1.0420 (5)	5.1 (2)
C8	1.1016 (5)	0.4372 (5)	0.9993 (5)	4.5 (2)
C20	0.9625 (5)	0.1262 (5)	0.9121 (5)	5.3 (2)
C21	0.8938 (5)	0.2539 (5)	0.8260 (6)	5.7 (2)
C10A	1.0828 (6)	0.1344 (7)	0.7260 (6)	1.1
C11A	1.0333 (8)	0.1997 (5)	0.6789 (6)	1.1
C12A	0.9408 (10)	0.1747 (10)	0.6697 (7)	2.5
C13A	0.9327 (11)	0.0882 (12)	0.7167 (11)	3.0
C14A	1.0234 (16)	0.0658 (8)	0.7487 (9)	2.9
C15A	1.1822 (11)	0.1412 (14)	0.7397 (11)	4.8 (5)
C16A	1.0704 (16)	0.2781 (12)	0.6381 (12)	4.9 (6)
C17A	0.8717 (14)	0.2148 (16)	0.6194 (14)	6.9 (7)
C18A	0.8583 (14)	0.0313 (15)	0.7244 (14)	8.1 (7)
C19A	1.0580 (18)	−0.0135 (10)	0.7957 (14)	6.5 (6)
C10B	1.0647 (17)	0.1670 (16)	0.7041 (16)	7.2
C11B	0.9869 (20)	0.1907 (13)	0.6727 (14)	6.8
C12B	0.9232 (10)	0.1288 (14)	0.6938 (12)	4.1
C13B	0.9693 (17)	0.0670 (8)	0.7359 (10)	3.4
C14B	1.0564 (16)	0.0832 (16)	0.7476 (14)	6.0
C15B	1.1714 (25)	0.1849 (23)	0.7173 (24)	5.0
C15C	1.1009 (29)	0.2659 (29)	0.6569 (29)	4.5
C16B	1.0147 (26)	0.2761 (26)	0.6229 (30)	6.4
C16C	0.8930 (30)	0.2577 (25)	0.6165 (32)	5.4
C17B	0.8363 (26)	0.1652 (24)	0.6460 (26)	6.0
C17C	0.8211 (25)	0.0847 (24)	0.6932 (27)	6.4
C18B	0.9054 (29)	−0.0104 (26)	0.7623 (28)	7.0
C18C	0.9959 (29)	−0.0203 (26)	0.7840 (28)	6.4
C19B	1.1072 (24)	0.0099 (24)	0.8004 (26)	5.0
C19C	1.1683 (35)	0.0997 (33)	0.7626 (34)	7.9
O1	0.9526 (5)	0.0909 (4)	0.9777 (4)	8.1 (2)
O2	0.8403 (4)	0.3046 (4)	0.8356 (5)	9.0 (2)

[a] CpA and CpB are the centroids of C10A–C14A and C10B,C–C14B,C, respectively.

Table VII. Selected Bond Lengths and Angles for Fp*—C≡C—Ph (1b)

	Bond Lengths, Å		
Fe1–CpA	1.734 (1)	C5–C6	1.380 (11)
Fe1–C1	1.924 (7)	C6–C7	1.362 (13)
Fe1–C20	1.757 (8)	C7–C8	1.376 (11)
Fe1–C21	1.747 (8)	C8–C3	1.396 (10)
Fe1–C(C10A–C14A)	2.145	C20–O1	1.135 (10)
C1–C2	1.214 (9)	C21–O2	1.150 (11)
C2–C3	1.431 (9)	C–C(C10A–C14A)	1.484
C3–C4	1.393 (10)	C(C10A–C14A)–Me	1.486
C4–C5	1.385 (11)		
	Bond Angles, deg		
CpA–Fe1–C1	122.89 (20)	C4–C3–C8	117.31 (59)
CpA–Fe1–C20	125.24 (25)	C3–C4–C5	120.74 (64)
CpA–Fe1–C21	124.70 (28)	C4–C5–C6	120.85 (73)
C1–Fe1–C20	89.44 (32)	C5–C6–C7	118.68 (73)
C1–Fe1–C21	87.78 (34)	C6–C7–C8	121.43 (73)
C20–Fe1–C21	96.50 (38)	C7–C8–C3	120.94 (69)
Fe1–C1–C2	175.89 (60)	Fe1–C20–O1	179.34 (98)
C1–C2–C3	175.46 (70)	Fe1–C21–O2	177.97 (75)
C2–C3–C4	122.57 (57)	C–C–C(C10A–C14A)	107.99
C2–C3–C8	120.11 (61)	C–C(C10A–C14A)–Me	125.91

[a] Lengths and angles without standard deviations are averaged values. CpA and CpB are the centroids of C10A–C14A and C10B,C–C14B,C, respectively.

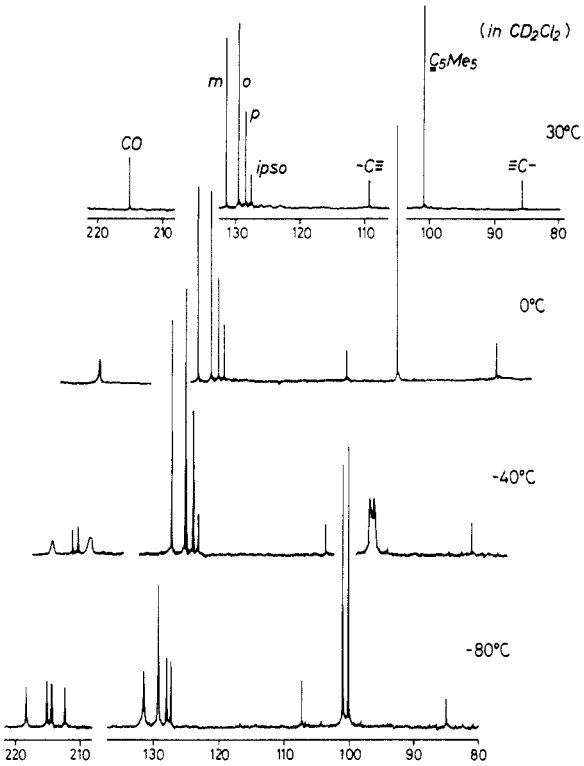

Figure 4. Variable-temperature ^{13}C NMR spectra of [Fp*$_2$(C≡C—Ph)]BF_4 (**2b**) observed at 68 MHz in CD_2Cl_2.

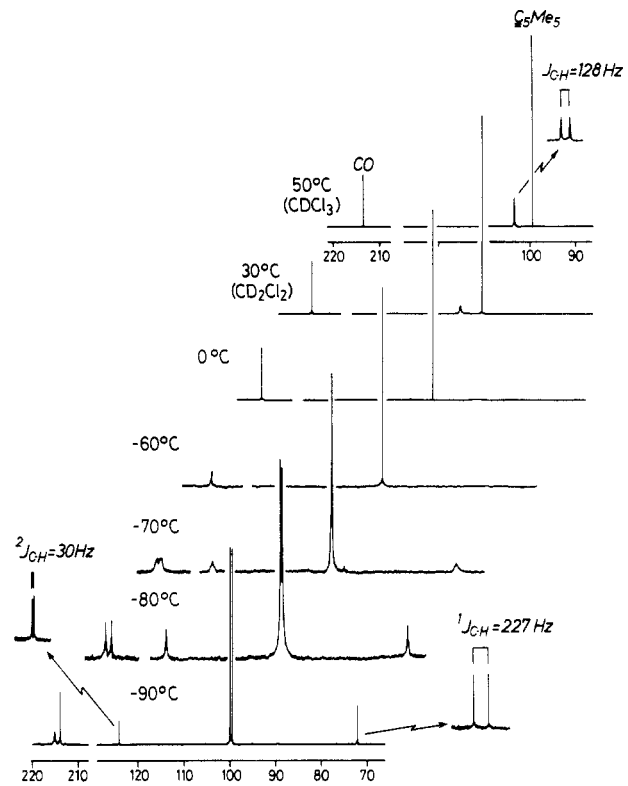

Figure 5. Variable-temperature ^{13}C NMR spectra of [Fp*$_2$(C≡C—H)]BF_4 (**2a**) observed at 68 MHz in $CDCl_3$ (50 °C) and CD_2Cl_2 (−90 to +30 °C).

Spectroscopic Characterization of Diiron μ-Acetylide Complexes 2. The decrease in bond order of the C≡C part brought about by coordination to a metal center is clearly demonstrated by IR. ν_{C-H} of the ethynyl ligand of **2a** and $\nu_{C\equiv C}$ of **2a–c** appear at lower frequencies than those of the starting complexes (**1**).

Fluxional behavior for **2** on the NMR time scale is evident, as reported for other dinuclear μ-acetylide complexes.[4] We initially observed ^1H NMR spectra at lower temperatures (Figure 3). While only one Cp* or Cp resonance was observed for all **2** at room temperature, it was split into two singlet signals below −50 °C (except in **2a**). The activation parameters estimated by line-shape analysis are as follows: **2b** (in CD_2Cl_2), $\Delta H^\ddagger$ = 8.9 kcal/mol, $\Delta S^\ddagger$ = −14.1 eu, $\Delta G^\ddagger$ (at 273 K) = 5.1 kcal/mol; **2c** (in acetone-d_6), $\Delta H^\ddagger$ = 9.1 kcal/mol, $\Delta S^\ddagger$ = −10.7 eu, $\Delta G^\ddagger$ (at 273 K) = 6.2 kcal/mol); **2d** (in acetone-d_6), $\Delta H^\ddagger$ = 8.4 kcal/mol, $\Delta S^\ddagger$ = −14.0 eu, $\Delta G^\ddagger$ = 4.6 kcal/mol. On cooling **2c** a ca. 2:1 equilibrium mixture of isomers, [Fp(Fp*—C≡C—Ph)]BF_4 and [Fp*(Fp—C≡C—Ph)]BF_4, was obtained. The major isomer is tentatively assigned to the former isomer on the basis of our previous work,[7c] but their structures cannot be assigned by NMR data alone. The Cp* signal of **2a** did not split even at −90 °C (at 100 MHz), but it was slightly broadened.

We then examined variable-temperature ^{13}C NMR of **2a** and **2b**. At room temperature the ^{13}C NMR spectrum of **2b** contains PhC≡C signals and only one set of Fp* signals (Figure 4). At about −40 °C Fp* signals split into two C_5Me_5 absorptions and four nonequivalent CO signals, and the limiting spectrum coincides with the solid-state structure (vide infra). The absorptions owing to the Ph—C≡C part did not change significantly over the observed temperature range (−80 to +30 °C). On the other hand, fluxional behavior of different type was observed for **2a** (Figure 5). The signals due to the C_5Me_5 and the CO groups split at −70 °C, but only two CO signals were observed at this temperature. Although the CO absorption at lower field broadened upon cooling the sample, rotation around the Fe–C bond was not frozen out even at −90 °C. In addition, the ethynyl ligand exhibited quite different behavior from the phenylethynyl ligand in **2b**. Splitting of the C≡CH signals was observed at the same temperature as for the Cp* signal, and the signal at higher field was readily assigned to C_β on the basis of $^1J_{C-H}$ value (227.0 Hz). Over the range of −60 to 0 °C the broad C≡CH signals could not be located, but a sharp signal emerged at 103.45 ppm when measured at 50 °C. Note that values of the chemical shift and the coupling constant (128 Hz) observed at 50 °C are approximately equal to averaged values of those of C_α and C_β signals observed at −90 °C [(124.18 + 72.22)/2 = 98.2 ppm, (29.7 + 227.0)/2 = 128.35 Hz]. These results suggest that the acetylenic proton interacts with two equivalent acetylenic carbon atoms at higher temperature; in other words, the proton moves between two acetylenic carbon atoms at a rate that is much faster than the NMR time scale. The activation parameters for this process estimated by the line-shape analysis are $\Delta H^\ddagger$ = 8.3 kcal/mol, $\Delta S^\ddagger$ = −8.6 eu, and $\Delta G^\ddagger$ (at 273 K) = 6.0 kcal/mol (in CD_2Cl_2).

Molecular Structures of Cationic Diiron μ-Acetylide Complexes 2a,b. The divergent fluxional behavior observed for **2a** and **2b** prompted us to determine their molecular structures by X-ray crystallography.

Crystallographic data, positional parameters, and selected bond lengths and angles are listed in Tables III and VIII–XI. ORTEP drawings are shown in Figures 6 (**2a**) and 7 (**2b**).

The overall geometries of **2a** and **2b** are in accord with the limiting structures, i.e., dinuclear μ-(η^1:η^2)-acetylide complexes, and are essentially the same, as is evident from the side views (Figures 6b and 7b). The Cp* ligands and

(12) March, J. W. *Advanced Organic Chemistry*; Wiley: New York, 1985.

Table VIII. Positional Parameters and B_{eq} (Å^2) for Non-Hydrogen Atoms of [Fp*$_2$—C≡C—H]BF$_4$ (2a)[a]

atom	x	y	z	B_{eq}
Cp1	0.73257	0.11020	1.25757	
Cp2	0.76272	0.13886	0.71491	
Fe1	0.76796 (5)	0.15782 (3)	1.15359 (6)	4.58 (2)
Fe2	0.72605 (5)	0.08703 (3)	0.81494 (6)	4.26 (2)
C1	0.6976 (3)	0.1434 (2)	0.9840 (4)	4.2 (2)
C2	0.6323 (4)	0.1420 (3)	0.8840 (4)	5.0 (2)
C3	0.8843 (4)	0.1499 (3)	1.1566 (4)	6.3 (2)
C4	0.7594 (4)	0.2607 (3)	1.1289 (5)	7.4 (2)
C5	0.6405 (4)	0.0094 (3)	0.7665 (4)	5.5 (2)
C6	0.8043 (4)	0.0288 (3)	0.9331 (4)	5.2 (2)
C10	0.6974 (4)	0.0565 (3)	1.1872 (4)	4.7 (2)
C11	0.7923 (4)	0.0598 (3)	1.2725 (4)	5.1 (2)
C12	0.8045 (4)	0.1333 (3)	1.3373 (4)	5.4 (2)
C13	0.7175 (4)	0.1735 (3)	1.2935 (4)	5.4 (2)
C14	0.6512 (4)	0.1280 (3)	1.1974 (4)	5.0 (2)
C15	0.6515 (5)	−0.0109 (3)	1.1038 (5)	6.6 (2)
C16	0.8639 (5)	−0.0058 (4)	1.2997 (6)	7.5 (2)
C17	0.8934 (5)	0.1590 (5)	1.4434 (6)	8.2 (3)
C18	0.6949 (5)	0.2494 (4)	1.3428 (6)	8.2 (3)
C19	0.5474 (5)	0.1474 (4)	1.1283 (6)	7.3 (3)
C20	0.6962 (4)	0.1122 (3)	0.6305 (4)	4.9 (2)
C21	0.7879 (4)	0.0761 (3)	0.6873 (5)	5.6 (2)
C22	0.8448 (3)	0.1279 (3)	0.7809 (4)	5.4 (2)
C23	0.7886 (4)	0.1938 (3)	0.7850 (4)	4.8 (2)
C24	0.6962 (4)	0.1842 (3)	0.6909 (4)	4.5 (2)
C25	0.6155 (5)	0.0815 (4)	0.5200 (5)	7.2 (2)
C26	0.8191 (6)	0.0002 (4)	0.6462 (7)	9.5 (4)
C27	0.9508 (5)	0.1188 (6)	0.8542 (7)	9.0 (3)
C28	0.8195 (5)	0.2646 (4)	0.8660 (6)	7.2 (3)
C29	0.6171 (5)	0.2440 (4)	0.6552 (6)	7.0 (3)
O1	0.9621 (3)	0.1446 (3)	1.1646 (4)	9.7 (2)
O2	0.7521 (4)	0.3277 (2)	1.1142 (4)	13.0 (3)
O3	0.5867 (3)	−0.0415 (2)	0.7342 (3)	8.1 (2)
O4	0.8579 (3)	−0.0107 (2)	1.0058 (3)	8.1 (2)
B1	0.3668 (5)	0.1353 (4)	0.6095 (6)	6.4 (3)
F1	0.3803 (2)	0.1291 (2)	0.5045 (3)	8.1 (1)
F2	0.4002 (3)	0.2075 (2)	0.6602 (4)	13.7 (2)
F3	0.4240 (3)	0.0822 (2)	0.6897 (3)	12.6 (2)
F4	0.2780 (2)	0.1258 (3)	0.5968 (3)	10.8 (2)

[a] Cp1 and Cp2 are the centroids of C10–C14 and C20–C24, respectively.

Table IX. Selected Bond Lengths and Angles for [Fp*$_2$—C≡C—H]BF$_4$ (2a)[a]

	Bond Lengths, Å		
Cp1–Fe1	1.732 (1)	C4–O2	1.141 (7)
Cp2–Fe2	1.738 (1)	C5–O3	1.144 (6)
Fe1–C3	1.755 (6)	C6–O4	1.147 (6)
Fe1–C4	1.756 (6)	C–C(C10–C14)	1.417
Fe1–C(C10–C14)	2.110	C(C10–C14)–Me	1.502
Fe2–C5	1.774 (5)	C–C(C20–C24)	1.420
Fe2–C6	1.755 (5)	C(C20–C24)–Me	1.504
Fe2–C(C20–C24)	2.117	B1–F	1.345
C3–O1	1.149 (8)		
	Bond Angles, deg		
Cp1–Fe1–C1	120.36 (15)	C2–Fe2–C5	86.26 (24)
Cp1–Fe1–C3	122.50 (17)	C2–Fe2–C6	106.05 (24)
Cp1–Fe1–C4	123.74 (24)	C5–Fe2–C6	91.92 (22)
C1–Fe1–C3	98.99 (23)	Fe1–C3–O1	176.65 (45)
C1–Fe1–C4	88.37 (20)	Fe1–C4–O2	178.30 (73)
C3–Fe1–C4	95.02 (29)	Fe2–C5–O3	178.45 (57)
Cp2–Fe2–C1	125.92 (11)	Fe2–C6–O4	176.03 (56)
Cp2–Fe2–C2	119.44 (14)	C–C–C(C10–C14)	107.98
Cp2–Fe2–C5	122.14 (18)	C–C(C10–C14)–Me	125.91
Cp2–Fe2–C6	122.74 (20)	C–C–C(C20–C24)	107.99
C1–Fe2–C5	102.73 (22)	C–C(C20–C24)–Me	125.90
C1–Fe2–C6	80.07 (21)	F–B1–F	109.40

[a] Lengths and angles without standard deviations are averaged values. For the data for the bridging part, see Table XII and Figure 8a. Cp1 and Cp2 are the centroids of C10–C14 and C20–C24, respectively.

the phenyl substituent are placed parallel to minimize the steric repulsions. The structure of Fp* portions in **2a** and

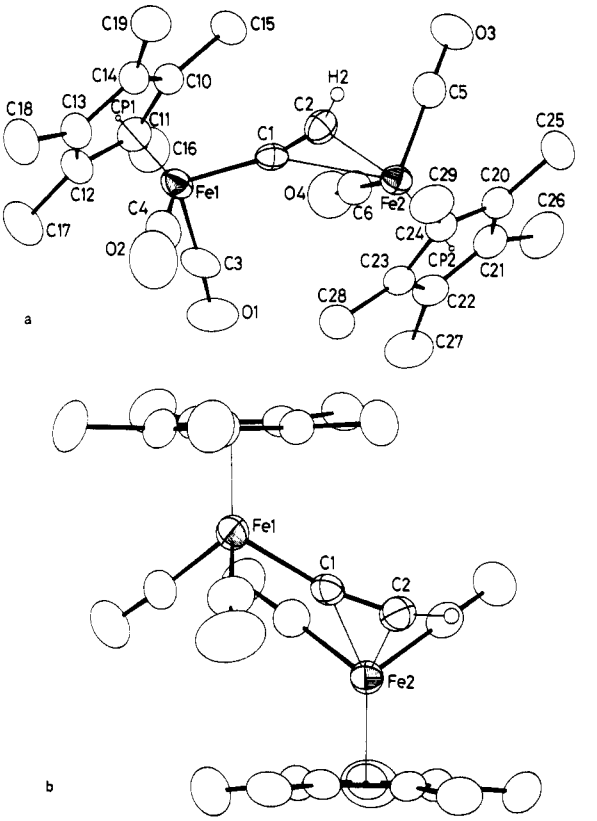

Figure 6. Molecular structure of [Fp*$_2$(C≡C—H)]BF$_4$ (**2a**) drawn at the 30% probability level: (a) perspective view; (b) side view.

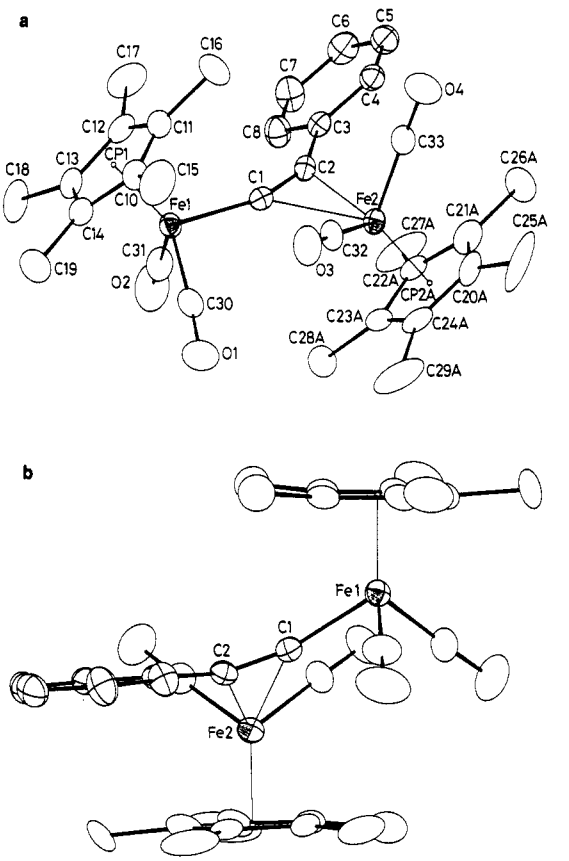

Figure 7. Molecular structure of [Fp*$_2$(C≡C—Ph)]BF$_4$ (**2b**) drawn at the 30% probability level: (a) perspective view; (b) side view.

2b is similar to that of **1a** and **1b**, and any systematic differences between neutral and cationic Fp* portions are not observed. The relation between molecular structure

Table X. Positional Parameters and B_{eq} (Å^2) of Non-Hydrogen Atoms for [Fp*$_2$—C≡C—Ph]BF$_4$ (2b)[a]

atom	x	y	z	B_{eq}
Cp1	0.63352	0.06207	0.48311	
Cp2A	1.06540	0.15421	0.85663	
Cp2B	1.06278	0.15112	0.86345	
Fe1	0.76276 (6)	0.06955 (2)	0.50888 (10)	2.77 (2)
Fe2	0.93659 (6)	0.14691 (2)	0.83703 (10)	2.83 (2)
C1	0.8263 (4)	0.1287 (2)	0.6109 (7)	2.7 (2)
C2	0.8475 (4)	0.1740 (3)	0.6333 (7)	2.8 (2)
C3	0.8393 (4)	0.2251 (2)	0.5737 (7)	2.9 (2)
C4	0.8372 (5)	0.2679 (3)	0.6623 (8)	3.4 (2)
C5	0.8331 (6)	0.3153 (3)	0.5993 (9)	4.2 (2)
C6	0.8307 (6)	0.3205 (3)	0.4422 (10)	4.7 (2)
C7	0.8322 (6)	0.2786 (3)	0.3501 (9)	4.9 (2)
C8	0.8358 (6)	0.2314 (3)	0.4141 (9)	4.2 (2)
C10	0.6384 (5)	0.0407 (3)	0.6046 (7)	3.6 (2)
C11	0.6250 (5)	0.0928 (3)	0.5817 (8)	3.9 (2)
C12	0.6247 (5)	0.1039 (3)	0.4218 (9)	3.9 (2)
C13	0.6346 (5)	0.0555 (3)	0.3468 (7)	3.8 (2)
C14	0.6449 (5)	0.0174 (3)	0.4606 (8)	3.5 (2)
C15	0.6337 (6)	0.0131 (4)	0.7548 (9)	6.6 (3)
C16	0.6087 (6)	0.1320 (3)	0.7026 (10)	6.6 (3)
C17	0.6050 (6)	0.1545 (3)	0.3450 (11)	6.6 (3)
C18	0.6276 (6)	0.0487 (3)	0.1743 (8)	6.4 (3)
C19	0.6483 (6)	−0.0390 (3)	0.4286 (10)	5.9 (3)
C20A	1.0658 (10)	0.1560 (9)	0.9952 (15)	4.1 (4)
C21A	1.0590 (9)	0.1983 (5)	0.8944 (27)	4.5 (4)
C22A	1.0613 (8)	0.1804 (8)	0.7428 (19)	3.6 (4)
C23A	1.0683 (10)	0.1259 (7)	0.7421 (22)	4.2 (5)
C24A	1.0725 (9)	0.1106 (6)	0.9086 (29)	4.6 (5)
C25A	1.0771 (10)	0.1528 (9)	1.1651 (13)	10.5 (8)
C26A	1.0598 (10)	0.2520 (5)	0.9536 (22)	8.1 (6)
C27A	1.0667 (8)	0.2161 (6)	0.6074 (17)	7.8 (5)
C28A	1.0769 (9)	0.0982 (7)	0.5965 (17)	8.0 (6)
C29A	1.0941 (9)	0.0554 (5)	0.9485 (24)	9.5 (7)
C20B	1.0649 (20)	0.1823 (13)	0.9613 (37)	3.1
C21B	1.0632 (23)	0.1922 (12)	0.8050 (43)	3.1
C22B	1.0675 (22)	0.1460 (15)	0.7297 (33)	2.3
C23B	1.0758 (24)	0.1037 (12)	0.8375 (41)	3.3
C24B	1.0726 (23)	0.1314 (14)	0.9838 (36)	3.2
C25B	1.0673 (22)	0.2210 (12)	1.0895 (36)	7.9
C26B	1.0711 (18)	0.2447 (10)	0.7393 (30)	5.6
C27B	1.0672 (21)	0.1401 (11)	0.5530 (33)	5.8
C28B	1.0873 (20)	0.0493 (11)	0.7813 (33)	6.8
C29B	1.0840 (19)	0.0932 (11)	1.1228 (32)	6.5
C30	0.8448 (5)	0.0232 (3)	0.5903 (8)	4.0 (2)
C31	0.8304 (5)	0.0827 (3)	0.3576 (8)	4.7 (2)
C32	0.8799 (5)	0.0909 (3)	0.8878 (7)	3.3 (2)
C33	0.8620 (5)	0.1827 (3)	0.9447 (7)	3.6 (2)
O1	0.8977 (5)	−0.0097 (2)	0.6393 (7)	7.1 (2)
O2	0.8720 (4)	0.0923 (3)	0.2570 (6)	8.1 (2)
O3	0.8468 (4)	0.0547 (2)	0.9276 (5)	5.2 (2)
O4	0.8147 (4)	0.2039 (2)	1.0223 (6)	6.2 (2)
B1	0.3654 (12)	0.1235 (5)	0.0069 (14)	7.0 (4)
F1A	0.3538 (20)	0.1077 (8)	0.1450 (18)	11.4 (8)
F2A	0.3014 (7)	0.1652 (4)	−0.0159 (10)	8.0 (3)
F3A	0.4565 (7)	0.1441 (6)	−0.0189 (13)	11.0 (5)
F4A	0.3337 (16)	0.0855 (5)	−0.0864 (17)	15.1 (7)
F1B	0.4423 (21)	0.0995 (11)	−0.0505 (30)	12.1
F2B	0.3939 (29)	0.1681 (12)	0.0084 (32)	14.8
F3B	0.3000 (20)	0.1115 (11)	−0.1041 (34)	9.9
F4B	0.3947 (35)	0.1065 (20)	0.1505 (55)	8.8

[a] Cp1, Cp2A, and Cp2B are the centroids of C10–C14, C20A–C24A, and C20B–C24B, respectively.

and fluxional behavior will be discussed later.

Discussion

Structure of Mononuclear Acetylide Complexes 1a and 1b. The iron atom in **1** is coordinated by one Cp* ligand and three isoelectronic C≡X ligands. The Fe–CO lengths are shortened by 0.17 Å compared with the Fe–C_2R lengths [1.921 Å (**1a**), 1.924 Å (**1b**)], which are even substantially shorter than the sum of covalent radii (1.99 Å) by 0.07 Å. [The covalent radius of the Fe atom in the Fp* group is estimated to be 1.29 Å according to the previous works.[11b]] The π-basic ligand with more electronegative oxygen atom effectively receives electrons through dπ–pπ back donation as reported by Fenske et al.,[13] and hence the M–CO bonds are considerably shortened by the increased double-bond character.

Table XI. Selected Bond Lengths and Angles for [Fp*$_2$—C≡C—Ph]BF$_4$ (2b)[a]

Bond Lengths, Å			
Cp1–Fe1	1.742 (1)	C5–C6	1.384 (12)
Cp2A–Fe2	1.738 (1)	C6–C7	1.377 (12)
Fe1–C30	1.740 (7)	C7–C8	1.371 (11)
Fe1–C31	1.756 (8)	C8–C3	1.408 (10)
Fe1–C(C10–C14)	2.123	C–C(C10–C14)	1.427
Fe2–C32	1.760 (7)	C(C10–C14)–Me	1.519
Fe2–C33	1.759 (7)	C–C(C20–C24)	1.429
Fe2–C(C20A–C24A)	2.130	C(C20–C24)–Me	1.510
C3–C4	1.379 (10)	B1–F	1.361
C4–C5	1.373 (10)		
Bond Angles, deg			
Cp1–Fe1–C1	121.35 (18)	C32–Fe2–C33	90.47 (33)
Cp1–Fe1–C30	122.81 (25)	C2–C3–C4	124.79 (58)
Cp1–Fe1–C31	123.25 (22)	C2–C3–C8	117.45 (58)
C1–Fe1–C30	99.62 (29)	C4–C3–C8	117.74 (62)
C1–Fe1–C31	86.86 (31)	C3–C4–C5	121.91 (66)
C30–Fe1–C31	94.60 (36)	C4–C5–C6	119.19 (71)
Cp2A–Fe2–C1	127.57 (16)	C5–C6–C7	120.49 (74)
Cp2A–Fe2–C2	118.83 (17)	C6–C7–C8	119.85 (75)
Cp2A–Fe2–C32	122.49 (22)	C7–C8–C3	120.82 (69)
Cp2A–Fe2–C33	122.21 (22)	C–C–C(C10–C14)	107.99
C1–Fe2–C32	78.15 (25)	C–C(C10–C14)–Me	125.86
C1–Fe2–C33	102.83 (25)	C–C–C(C20A–C24A)	108.00
C2–Fe2–C32	106.45 (26)	C–C(C20A–C24A)–Me	125.84
C2–Fe2–C33	88.39 (27)	F–B1–F	109.39

[a] Lengths and angles without standard deviations are averaged values. For the data for the bridging part, see Table XII and Figure 8b. Cp1, Cp2A, and Cp2B are the centroids of C10–C14, C20A–C24A, and C20B–C24B, respectively.

In addition, the dihedral angle between the Cp1–Fe1–C3 plane and the Cp1–Fe1–C4 plane in **1a** (129°) is slightly larger than the remaining two dihedral angles between Cp1–Fe1–C1 and –C3 (116°) and between Cp1–Fe1–C1 and –C4 (115°), in order to compensate for dipole moment of two CO ligands (Figure 1b). The same situation is observed in **1b**. The corresponding dihedral angles are 131°, 113°, and 116°.

Structure of Cationic Diiron μ-Acetylide Complexes 2. Organometallic reactions involving the C≡C group as a nucleophile can be divided into two types as shown in eqs 3 and 4.[1] The interaction of the first type

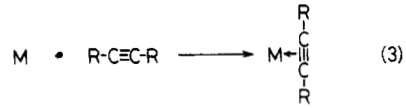

(3)

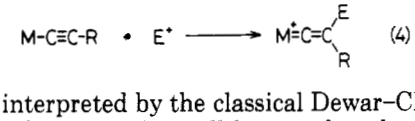

(4)

has been interpreted by the classical Dewar–Chatt–Duncanson model. It is also well-known that the metal acetylide complex is activated as a nucleophile by back-donation from the metal center and readily reacts with electrophiles at the β carbon to give a cationic vinylidene complex.[2] The cationic diiron μ-acetylide complex **2** prepared by us is intermediate between these two extremes.

A variety of limiting structures shown in Chart I are available for **2**. A is a π-bonded form. B and C are σ-bonded forms. D and E are plausible only when R = H (**2a**), but D should be energetically more favorable than E because of the high-lying orbital of the C≡C bond.

Contribution by A should result in the smallest difference in the two M2–C(acetylide) distances. In typical η^2-acetylene complexes the distances are almost equal (see

(13) Kostic, N. M.; Fenske, R. F. *Organometallics* **1982**, *1*, 974.

Table XII. Structural Parameters of the Bridging Part of Dinuclear μ-Acetylide Complexes[a]

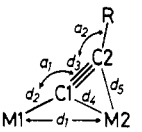

complex	d_1	d_2	d_3	d_4	d_5	a_1	a_2	$d_4 - d_2$	$d_5 - d_4$	$360 - (a_1 + a_2)$
2a	4.038	1.912	1.226	2.422	2.114	162.0	152	0.510	−0.308	46
2b	4.012	1.944	1.244	2.357	2.134	158.2	147.2	0.413	−0.223	54.6
2W	4.216	2.19	1.30	2.21	2.10	146	148	0.02	−0.11	66
CuMn	3.472	2.03	1.24	2.08	2.08	171	164	0.05	0.00	26
2Rh	3.155	2.043	1.182	2.209	2.616	168.0	172.9	0.166	0.407	19.1
PtRh	3.066	1.95	1.21	2.22	2.46	177	166	0.27	0.24	17
2Pt	2.703	1.96	1.26	2.14	2.47	171	163	0.18	0.33	26
2Fe	2.596	1.905	1.223	2.123	2.326	162.4	161.1	0.218	0.203	36.5
Pt			1.255	2.024	2.031	140.6	139.6		0.007	79.8
Fe			1.19	2.114	2.165	157.7	158.4		0.051	75.4

[a] d_1–d_5 are in angstroms. a_1 and a_2 are in degrees. 2W: $[W_2Cp_2(CO)_4(PhC_2H)(\mu\text{-}C_2Ph)]BF_4$.[4e] MnCu: $[Cu[Mn(CO)_3(dppe)(\mu\text{-}C_2Bu^t)]_2]BF_4$.[4j] 2Rh: $[Rh_2(CO)_2(\mu\text{-dppm})_2(\mu\text{-}C_2Bu^t)]ClO_4$.[4i] PtRh: $[PtRhCl(\mu\text{-dppm})_2(\mu\text{-}C_2Me)]BF_4$ [Pt–Rh].[4g] 2Pt: $Pt_2(PCy_3)_2(C_2Ph)(\mu\text{-}SiMe_2)(\mu\text{-}C_2Ph)$ [Pt–Pt].[4d] 2Fe: $Fe_2(CO)_6(\mu\text{-}PPh_2)(\mu\text{-}C_2Bu^t)$ [Fe–Fe].[4a] Pt: $Pt(PPh_3)_2(CF_3C_2CF_3)$. Davies, B. W.; Payne, N. C. *Inorg. Chem.* **1974**, *13*, 1848. Fe: Reger, D. L.; Klaeren, S. A.; Lebioda, L. *Organometallics* **1988**, *7*, 189.

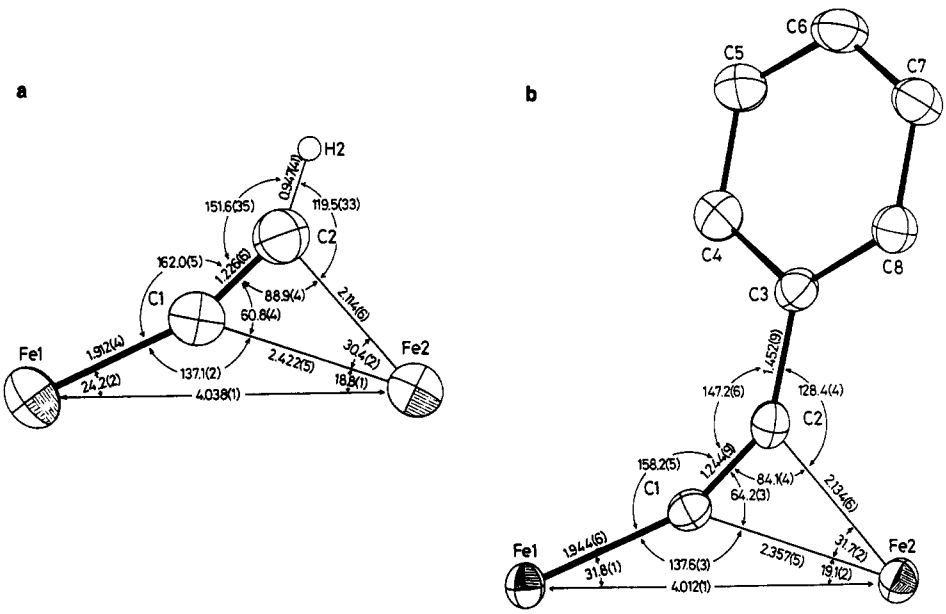

Figure 8. Structure of the bridging part of **2a** (a) and **2b** (b).

Chart I

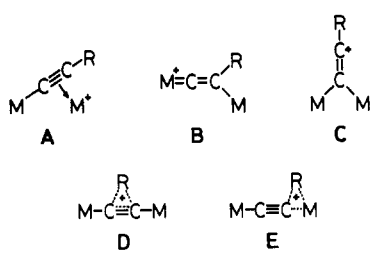

Pt and Fe in Table XII). On the other hand, when B or C dominates, a considerable difference in M2–C(acetylide) distances should be observed. In addition, the α carbon in B should resonate in very low field (>300 ppm) characteristic of vinylidene carbons.

The detail structure of the bridging part of **2a** and **2b** is shown in Figure 8. The structural parameters of **2a** and **2b** are compared with those of hitherto reported dinuclear μ-acetylide complexes (Table XII).

Since two metal centers in the reference complexes (except the MnCu and the 2W complexes) are linked by additional bridging ligands or a metal–metal bond, the metal–metal separation (d_1) and the difference in distances from C1 to the two metal atoms ($d_4 - d_2$) are much smaller than those of **2a** and **2b**. Of the structural parameters listed in Table XII the difference in distances from M2 to C2 and C1 ($d_5 - d_4$) is the most striking. In the reference complexes C1 lies closer to M2 than C2 by 0.2–0.4 Å. Although this structural feature may result in part from the steric constraint brought about by the two metal centers being put closer owing to the additional interactions, even for the MnCu complex, for which any additional bridging interaction other than the acetylide ligand is not available, d_4 does not exceed d_5. In addition, the sum of bend-back angles $[360 - (a_1 + a_2)]$, which is regarded as an index of deviation from the linearity of the acetylide ligand, i.e., the extent of coordination [0° for free acetylene, 120° for an ideal η^2-acetylene complex, and 60° for an ideal vinylidene complex], is smaller than 40° for the reference complexes, perhaps because the optimum orbital interactions are prevented by the above-mentioned steric constraint.

For **2a**, **2b**, and the 2W complex opposite or different features are apparent, as shown in Table XII. The β carbon of the acetylide ligand lies closer to the M2 atom ($d_5 - d_4 < 0$) and the sum of bend-back angles are larger than those of the reference complexes. The structural

Scheme I

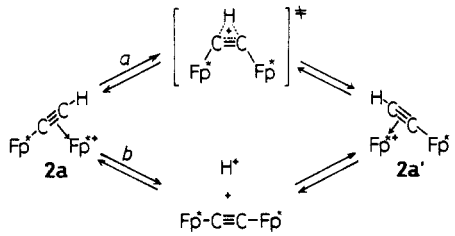

Scheme II

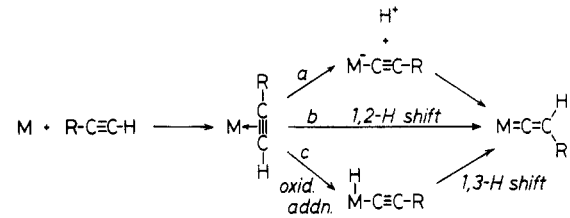

features observed for the present cationic diiron μ-acetylide complexes **2a**, **2b**, and the 2W complex [$d_4 \gg d_2$, $d_4 > d_5$, $360 - (a_1 + a_2) = 46°$ (**2a**), 55° (**2b**), 66° (2W)] are best interpreted by the contribution of the vinylidene complex form (B) in addition to the dominant contribution of the π-complex (A). In accord with this consideration, C_α in **2a** appears in lower field than C_β (nearer to the vinylidene carbon region). The acetylenic carbons of **2b**, **2c**, and **2d** resonating in lower field are tentatively assigned to C_α.

When the structures of the bridging part of **2a** and **2b** are compared in detail, the following features are evident (Figure 8): (i) Fe1–Fe2, **2a** > **2b** (0.022 Å) [B > A]; (ii) Fe1–C1, **2a** < **2b** (0.022 Å) [B < A]; (iii) C1–C2, **2a** < **2b** (0.018 Å) [B > A]; (iv) $d_1 - d_2$, **2a** > **2b** (0.097 Å) [B > A]; (v) $d_4 - d_5$, **2a** > **2b** (0.085 Å) [B > A]; (vi) $360 - (a_1 + a_2)$, **2a** < **2b** (8.6°) [B < A]. (Differences are shown in parentheses.) The same tendencies are observed for both **2a**–**2b** and B–A pairs with the exception of iii. Above all, the shortened Fe1–C1 length and the enlarged difference in $d_4 - d_5$ clearly demonstrate that the contribution of B plays a more important role in **2a** than in **2b**.

Thus, in the case of *cationic dinuclear μ-acetylide complexes in which two metal centers are connected only by a μ-(η^1:η^2)-acetylene ligand* (**2a**, **2b**, and 2W) the above-mentioned structural features are brought about by the synergistic electronic and steric effects (repulsion between two metal fragments).

Fluxional Behavior of [FP$_2$(C≡C—R)]BF$_4$ (2). The fluxional behavior of **2b** is consistently explained by the "wiper"-like oscillation process, which has been observed for homodinuclear μ-acetylide complexes.[4] A plausible mechanism for the fluxional process is shown in eq 5.[14]

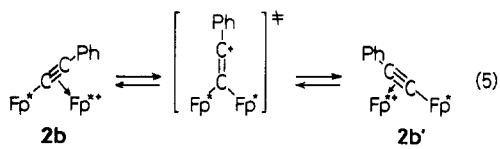

(5)

2b **2b'**

The electrons used for the π-bond flow into the M–C σ-bond orbital, and in the transition state a positive charge is developed at the β-position to generate a free vinyl cation, which should be stabilized by conjugation with the π-electrons of the phenyl group. Successive coordination to either of the two metal centers regenerates **2b**. Throughout this process the α carbon retains an interaction with both metal centers. Hence, the contribution of C, which has never been detected by spectroscopic and structural analyses, becomes apparent by observation of a dynamic process.

On the other hand, the fluxional process observed for **2a** involves proton migration,[15] and two mechanisms are proposed (Scheme I). In the first mechanism (a) the proton moves between two acetylide carbon atoms with retention of contact with them. The second mechanism (b) includes a fast deprotonation–reprotonation equilibrium. These two processes can be discriminated by the reaction with bases. The action of NaOMe to **2a** resulted in formation of Fp*—C≡C—Fp* (eq 6),[16] and protonation

$$[Fp^*_2(C{\equiv}C{-}H)]BF_4 + NaOMe \xrightarrow[THF]{} Fp^*{-}C{\equiv}C{-}Fp^* \quad (6)$$

1a

of the resulting Fp*—C≡C—Fp* with CF_3SO_3H regenerated **2a** (a $CF_3SO_3^-$ salt) (eq 7).[16] Whereas these ob-

$$Fp^*{-}C{\equiv}C{-}Fp^* + HOTf \xrightarrow[CH_2Cl_2]{} [Fp^*_2(C{\equiv}C{-}H)]OTf \quad (7)$$

$$TfO = CF_3SO_3$$

servations seem to suggest that the second mechanism is correct, treatment of **2a** with *n*-BuLi, *t*-BuLi, or LiHBEt$_3$ did not produce Fp*—C≡C—Fp* but afforded products in which the C–H bond originating from the C≡C—H part is retained.[16] Therefore, the second mechanism (Scheme I, b) is ruled out by the observation that **2a** cannot be deprotonated by stronger bases. According to the first mechanism (a), it should be noted that the carbon atom originally located at the α position in **2a** moves to the β position in **2a'** and that the transition state like D is completely different from that of **2b**.

The mechanism proposed for the fluxional process of **2a** may provide a clue to the problem of the formation of a vinylidene complex from a terminal acetylene and a metal complex.[2] A few reaction pathways shown in Scheme II have been proposed for the formation of a vinylidene complex. The metal center initially interacts with the π-electrons of terminal acetylene to give a η^2-acetylene complex. Deprotonation giving an acetylide complex followed by reprotonation at the β carbon (path a) or direct 1,2-shift of the acetylenic proton (path b) affords the vinylidene complex. When M is a coordinatively unsaturated species such as square-planar Rh(I) complexes, an alternative reaction pathway becomes available.[17] Successive oxidative addition of the C–H bond and 1,3-hydride migration also (path c) afford the product. If R and M are replaced with Fp* and Fp*$^+$, respectively, the η^2-acetylene complex and the vinylidene complex in Scheme II correspond to the possible limiting structures of **2a**, A and B. Then the structural change observed during the fluxional process of **2a** should correspond to the 1,2-proton shift mechanism (path b). Thus the present work is consistent with a 1,2-proton shift mechanism for the formation of a cationic vinylidene complex from a terminal acetylene and a cationic metal complex.

(14) Dyke, A. F.; Knox, S. A. R.; Morris, M. J.; Naish, P. J. *J. Chem. Soc., Dalton Trans.* **1983**, 1417.

(15) Preparation of [[(OC)$_5$Re]$_2$(C≡C—H)]BF$_4$, a rhenium analogue of **2a**, was already reported by Beck.[5f] The $^1J_{C-H}$ value (134 Hz) of the ethynyl ligand similar to that of **2a** (126.7 Hz) also suggests the occurrence of a similar fluxional process, but variable-temperature NMR analysis was not examined.

(16) Akita, M.; Terada, M.; Moro-oka, Y., manuscript in preparation.

(17) Hohn, A.; Otto, H.; Dziallas, M.; Werner, H. *J. Chem. Soc., Chem. Commun.* **1987**, 852.

Experimental Section

All manipulations were conducted under argon atmosphere by using standard Schlenk tube techniques. Analytical facilities have been described in our previous paper.[18] Solvents were dried over appropriate drying agents, distilled, and stored under argon. THF (tetrahydrofuran), ether, hexane:Na/K benzophenone; CH_2Cl_2:P_2O_5. Deuterated solvents for NMR measurements were dried over molecular sieves and distilled in vacuo before use. Column chromatography was carried out on alumina (Merck Art. 1097). Lithium acetylide–ethylenediamine complex, phenylacetylene, and *n*-BuLi were purchased from Kanto Chemicals, Tokyo Chemical Industry, and Aldrich, respectively, and used as received. $[Fp^+(THF)]BF_4$ was prepared according to the published method.[7a] Fp*I was prepared by the reaction of Fp^*_2 with I_2 in CH_2Cl_2 at room temperature.[19] $[Fp^{*+}(THF)]BF_4$ was prepared by the treatment of Fp*I with $AgBF_4$ in THF followed by recrystallization from CH_2Cl_2–ether.[7b]

Preparation of Fp*—C≡C—H (1a). Lithium acetylide–ethylenediamine complex (1.15 g, 12.48 mmol) was suspended in THF (50 mL) and cooled at −78 °C. Fp*I (3.59 g, 9.60 mmol) was added to the suspension in small portions. After 5 min the reaction mixture was gradually warmed to room temperature, and the stirring was continued overnight at the same temperature. The completion of the reaction being checked by TLC (alumina), the excess lithium acetylide was destroyed by the addition of MeOH (1 mL). The volatiles were then removed under reduced pressure, and the products were extracted with ether. After removal of inorganic salts by filtration through an alumina pad, the products were isolated by column chromatography. Fp^*_2 and Fp*I were eluted at first (CH_2Cl_2:hexane = 1:5–4). Elution of the dark green band with CH_2Cl_2:hexane = 1:3–1 followed by recrystallization from ether–hexane gave Fp*—C≡C—H (**1a**, 1.09 g, 4.00 mmol, 42%) as yellow plates, mp 112 °C. Anal. Calcd for $C_{19}H_{16}O_2Fe$: C, 61.82; H, 5.88. Found: C, 61.52; H, 5.65. FDMS 272 (M^+).

Preparation of Fp*—C≡C—Ph (1b). *n*-BuLi (1.67 M hexane solution, 19.8 mL, 32.1 mmol) was added dropwise to a THF solution (30 mL) of PhC≡CH (4.10 mL, 37.5 mmol) cooled at −78 °C. After 5 min the cooling bath was removed, and the mixture was stirred for 40 min at room temperature. The solution was recooled at −78 °C, and Fp*I (4.00 g, 10.70 mmol) was added to the mixture in small portions. After 5 min the reaction mixture was gradually warmed to room temperature and stirred for 1 h. Then the excess lithium reagent was destroyed by the addition of MeOH (2 mL), and the volatiles were removed under reduced pressure. The excess PhC≡CH was washed out with hexane (20 mL × 2). Ether extraction of the product from the residue and filtration through an alumina pad followed by recrystallization from ether–hexane gave Fp*—C≡C—Ph (**1b**, 2.42 g, 6.95 mmol, 65%) as orange-yellow needles, mp 126–127 °C. Anal. Calcd for $C_{25}H_{20}O_2Fe$: C, 73.55; H, 4.94. Found: C, 73.62; H, 4.92. FDMS 348 (M^+).

Preparation of $[Fp^*_2(C{\equiv}C{-}H)]BF_4$ (2a). Fp*—C≡C—H (1.23 g, 4.15 mmol) and $[Fp^{*+}(THF)]BF_4$ (1.43 g, 3.53 mmol) were stirred overnight in dichloromethane (40 mL). The volatiles were evaporated and the residue was washed with ether (10 mL × 2). Extraction with dichloromethane, filtration through a Celite pad, and addition of ether gave $[Fp^*_2(C{\equiv}C{-}H)]BF_4$ (**2a**, 1.75 g, 2.89 mmol, 82%) as dark brown precipitates, mp 150 °C. Anal. Calcd for $C_{36}H_{31}O_4Fe_2BF_4$: C, 51.55; H, 5.12. Found: C, 51.27; H, 4.94.

Other cationic diiron μ-acetylide complexes were similarly prepared. $[Fp^*_2(C{\equiv}C{-}Ph)]BF_4$ (**2b**), 82%, mp 203 °C. Anal. Calcd for $C_{42}H_{35}O_4Fe_2BF_4$: C, 56.37; H, 5.13. Found: C, 56.26; H, 5.27. $[FpFp^*(C{\equiv}C{-}Ph)]BF_4$ (**2c**) 68% from **1b** and 73% from **1c**, mp 130 °C. Anal. Calcd for $C_{27}H_{25}O_4Fe_2BF_4$: C, 53.14; H, 4.13. Found: C, 53.20; H, 4.15. $[Fp_2(C{\equiv}C{-}Ph)]BF_4$ (**2d**), yield 48%. **2d** was obtained as a dark brown tarry solid, and an analytically pure sample could not be obtained.

Single-Crystal X-ray Diffraction Studies. Suitable crystals of **1a,b** and **2a,b** were obtained by repeated recrystallization from ether–hexane and CH_2Cl_2–ether mixing solvent systems, respectively, and mounted on glass fibers. Diffraction measurements were made on a Rigaku AFC-5 automated four-circle diffractometer by using graphite-monochromated Mo Kα radiation (λ = 0.71058 Å). Unit cells were determined and refined by a least-squares method using 25 independent reflections with 25° < 2θ < 30°. Data were collected with ω–2θ scan technique and the scan speed was 6°/min. If $\sigma(F)/F$ was more than 0.1, a scan was repeated up to three times and the results were added to the first scan. Three standard reflections were monitored at every 100 measurements. Crystal data, data collection parameters, and results of the analyses are listed in Table III. All data processing was performed on a FACOM A-70 computer by using the R-CRYSTAN structure solving program system obtained from the Rigaku Corp., Tokyo, Japan. Neutral scattering factors were obtained from the standard sources.[20] In the reduction of data, Lorentz and polarization corrections were made and no absorption correction was made. Full-matrix least-squares refinement minimized the function $[\sum w(|F_o| - |F_c|)^2/\sum w|F_o|^2]^{1/2}$, where $w = 1/[\sum(F_o)^2 + (pF_o)^2]$, the parameter p being automatically optimized.

1a, **2a**, and **2b** were crystallized in a monoclinic system and **1b** in a orthorhombic system. The positions of Fe atoms were located by the direct method. Subsequent difference Fourier map revealed the positions of all non-hydrogen atoms. For **1a** and **2a** all non-hydrogen atoms were refined with anisotropic thermal parameters and all hydrogen atoms with isotropic thermal parameters. During refinement of the structures of **1b** and **2b** it became apparent that there was disorder in the C_5Me_5 and BF_4 parts as indicated by very large temperature factors. For **1b** three different disorder components [2(A):1(B):1(C)] were allowed for the methyl groups. But the positions of the ring carbons could not be resolved, and only two sets [1(A):1(B)] of the C_5 ring were found by the difference Fourier map. Then all the ring carbons, the methyl carbons of B and C groups, and the hydrogen atoms on the phenyl group were refined with isotropic thermal parameters and the other non-hydrogen atoms with anisotropic thermal parameters. For **2b** occupancy factors were adjusted to result in approximately equal thermal parameters for the resolved atom pairs and were determined to be 65:35. Anisotropic thermal parameters were used for refinement of the non-hydrogen atoms of the C_5Me_5 part and the BF_4 part of the major component and the other non-hydrogen atoms, and isotropic thermal parameters were used for refinement of those of the minor component and the hydrogen atoms on the phenyl ring.

Acknowledgment. We are grateful to Prof. Hiroshi Kihara (Hyogo University of Teacher Education) for providing us with an NMR simulation program. This work was financially supported by the Ministry of Education, Science, and Culture of the Japanese Government (Grant in Aid for Cooperative Research No. 63303009).

Note Added in Proof. After submission of this paper reports on an ethynylrhodium complex[21] and an Fe–Re μ-(η^1:η^2)-acetylide complex[22] appeared.

Supplementary Material Available: Tables of atomic coordinates, anisotropic thermal parameters, and bond lengths and angles and numbering schemes for the disordered parts (29 pages); a listing of structure factors (72 pages). Ordering information is given on any current masthead page.

(18) Akita, M.; Kondoh, A.; Kawahara, T.; Takagi, T.; Moro-oka, Y. *Organometallics* **1988**, *7*, 366.
(19) King, R. B. *Organometallic Synthesis*; Academic Press: New York, 1965; Vol. 1, p 175.
(20) *International Tables for X-Ray Crystallography*; Kynoch Press: Birmingham, 1975; Vol. 4.
(21) Bianchini, C.; Masi, D.; Meli, A.; Peruzzini, M.; Ramirez, J. A.; Vacca, A.; Zanobini, F. *Organometallics* **1989**, *8*, 2177.
(22) Fritz, P. M.; Polborn, K.; Steimann, M.; Beck, W. *Chem. Ber.* **1989**, *122*, 889.